Theoretical Study of the Mechanism of Corrosion Inhibition of Carbon Steel in Acidic Solution by 2-aminobenzothaizole and 2-Mercatobenzothiazole

Roqaya H. Albrakaty[1], Nuha A. Wazzan[1,], and I. B. Obot[2]*

[1] King Abdulaziz University, College of Science, Chemistry Department, Jeddah, Saudi Arabia
[2] Centre of Research Excellence in Corrosion, Research Institute, King Fahd University of Petroleum and Minerals, Dhahran 31261, Saudi Arabia
[*]E-Mail: nwazzan@kau.edu.sa

The purpose of the present study is to provide atomic-level understanding of the mechanism of corrosion inhibition of two well-known corrosion inhibitors, 2-aminobenzothiazole (ABT) and 2-mercaptobenzothiazole (MBThione), for steel in acidic media. Quantum chemical calculations and Monte Carlo simulations were the theoretical tools adopted for this study. The two inhibitors can exist in different tautomeric forms and can be protonated at different positions. Thus, quantum chemical calculations of two methods (B3LYP and MP2) with two basis sets (6-311++G(d,p) and 6-311++G(3df,2p)) were used to calculate the electronic properties of the two molecules in their different tautomeric and protonated forms. The quantitative quantum chemical parameters were correlated with experimentally determined inhibition efficiencies. Next, a correlational study addresses the relationship between the quantum chemical parameters of five electronic states and the experimentally measured inhibition efficiencies (%IE). The results support the mixed mode of adsorption, *i.e.*, chemisorption (the chemical model based on bonding between inhibitor and metal), preceded by physisorption (electrostatic attraction between heteroatoms and metal). Monte Carlo simulations were further applied to identify the equilibrium adsorption configurations and to compute the adsorption energy between the diazole corrosion inhibitors and the Fe surface. The results indicate that the adsorption energies follow the order: MBThione > ABT. The efficiency order and the mechanism of action of the studied inhibitors on a steel surface, as obtained by experimental results, have been verified by theoretical calculations.

1. INTRODUCTION

In many reports, the potential of benzothiazole derivatives as anti-corrosives for metal surfaces in acidic medium has been investigated experimentally, with different electrochemical techniques, and computationally, with different quantum chemical approaches [1-4]. Quantum chemical calculations have proved to be a potent tool for investigating the mechanism of corrosion inhibition [1]. Jafari et al. studied the corrosion of ST-37 carbon steel in 1.0 M HCl solution using two benzothiazole derivatives: 2-mercaptobenzothiazole and 2-aminobenzothiazole. The investigation was performed by applying electrochemical impedance spectroscopy (EIS). Both inhibitors showed an excellent ability to prevent the corrosion of carbon steel in an acidic medium. The inhibition efficiency of 2-mercaptobenzothiazole is better than the performance of 2-aminobenzothiazole, which was supported by the ability of 2-mercaptobenzothiazole to be readily protonated and thus adsorbed more rapidly on a steel surface [2]. Patel et al. studied the corrosion inhibition of three derivatives of benzothiazole derivatives, namely, 2-aminobenzothiazole (ABT), 6-methyl-1,3-benzothiazol-2-amine (MABT) and 2-amino-1,3-benzthiazole-6-thiol (TABT) on mild steel in 1.0 N HCl solutions. Potentiodynamic polarization, weight loss, EIS, and linear polarization techniques were applied to evaluate the potential of the aforementioned molecules as potential corrosion inhibitors. In addition to their excellent performance, it was observed that these molecules act as mixed mode inhibitors, while an increase in their concentrations increased their percent inhibition efficiencies (%IE) in the following order: TABT > MABT > ABT [5]. Dehdab et al. followed this study with a theoretical investigation of these chemicals' corrosion inhibition using quantum chemical parameters (QCPs) in the gas phase and aqueous solutions at the B3LYP/6-311++G(d,p) level of theory [4]. The QCPs correlated very well with the %IEs, *i.e.,* the order of inhibition efficiency, predicted theoretically, was consistent with that obtained experimentally. From Mulliken charges and Atom-in-Molecule (AIM) analysis, the nature of the interaction between the inhibitor molecule and the iron surface was predicted to be covalent and partially electrostatic [4]. In combined experimental and theoretical calculations, Danaee et al. investigated the anti-corrosive properties of ABT in different tautomeric forms of steel in 1.0 M H_2SO_4 solutions using electrochemical techniques and quantum chemical calculations, and a correlation between the QCPs of the tautomeric forms of the molecule with their experimental %IEs was achieved [1]. Additionally, in a combined experimental and theoretical (using B3LYP/6-311G (d,p)) investigation of five urea derivatives, Elshakre et al. found a correlation between the QCPs and five different electronic states of these derivatives. According to this correlation, the chemical adsorption of the inhibitor molecules on the metal surface was the predominant adsorption model compared to the physical model of adsorption [6].

Additionally, molecular dynamic simulations (MDS) and Monte Carlo (MC) simulations were also used along with DFT methods by several researchers to investigate the mechanism of adsorption of inhibitor molecules on metal surfaces. For instance, Oguzie et al. used DFT calculations to simulate the electronic structures of some extracted constituents of P. guineense (PG) leaves on mild steel corrosion in acidic solutions [7]. The chemisorptive interaction between the piperine molecule (the active constituent of the extract) and the Fe (110) surface was modelled by quantum chemical computations. The value of the calculated adsorption energy suggests strong chemisorption of the

piperine molecule, a result that was proven experimentally. Belghiti et al., by applying the EIS and potentiodynamic polarization techniques, studied the anticorrosive properties of two newly discovered benzylidene-aniline derivatives for carbon steel in HCl solution [8]. After demonstrating the good inhibition effect of the two investigated molecules for different factors affecting their %IEs, these researchers used quantum chemical calculations using DFT to investigate the effect of molecular structure on inhibition efficiency. The best configurational space for the two inhibitors on $Fe_2O_3(1\ 1\ 1)$ systems was investigated by a Monte Carlo simulation technique. The results from MDS correlated notably well with the experimental findings on the order of inhibition efficiencies and also correlated with the adsorption energies. Kaya et al. investigated the corrosion inhibitive performance of biologically active amino acids, such aspartate alanine, lysine, asparagine, and methionine. [9]. MDS were used to locate the minimum energy configuration and binding energies for the interaction of the amino acid corrosion inhibitors on the Cu (111)/50 H_2O interface. These findings correlated very well between the theoretical and the experimental data. The adsorption and corrosion inhibition properties of several novel quinoline derivatives has been studied theoretically by Erdoğan et al. [10]. The adsorption behaviours of studied inhibitors on the Fe (110) surface were investigated with the use of an MDS approach. The calculated binding energies of the investigated inhibitors on the Fe (110) surface correlated well with their experimental inhibition efficiencies.

In this report, a systematic study was conducted using the DFT and MP2 calculations and two basis sets (6-311++G(d,p) and 6-311++G(3df,2p)) of the most stable tautomeric forms of 2-aminobenzothiazole (ABT) and 2-mercaptobenzothiazole (MBThione). Correlations were investigated between the small differences in molecular structure of different tautomers with their inhibition efficiencies. The kinetics and thermodynamics of the tautomeric processes were also calculated. Additionally, the possible protonated forms and thus the proton affinities of the two inhibitors were simulated, and their stabilities were compared. A correlational study was conducted to address the relationship between the quantum chemical parameters of five electronic states and their experimentally measured inhibition efficiencies (%IE), for the corrosion of carbon steel in acidic solution. Monte Carlo simulations were further applied to identify the equilibrium adsorption configurations and to compute the adsorption energy between the diazole corrosion inhibitors and the Fe surface. The results indicate that the adsorption energies follow the order: MBThione > ABT. In strong agreement with the experimental data, the theoretical results also showed the order of inhibitory efficiency to be MBThione > ABT.

2. COMPUTATIONAL DETAILS

2.1. Ab initio methods

Calculations were performed using the Gaussian 09 suite of programmes [11]. Geometry optimizations were conducted by DFT using Becke's three parameter exchange functional,[12] the Lee–Yang–Parr correlation functional (B3LYP),[13] and the second-order Møller-Plesset [14] with split-valence triple zeta basis sets with different polarization functionals, 6-311++G(d,p) and 6-

311++G(3df,2p). In geometry optimizations, every geometrical parameter was allowed to relax, free of any constraints. The nature of the stationary points (*i.e.*, whether the obtained point is a minimum or a saddle point on the potential energy surface) was confirmed by vibrational frequency analysis, and only points with no imaginary frequency were considered for all geometries.

Frontier molecular orbitals (FMO); highest occupied molecular orbital (HOMO) and lowest unoccupied molecular orbital (LUMO) were used to predict the adsorption active site/s of the inhibitor molecules. Absolute electronegativity, χ, and absolute hardness, η, are given by [15]

$$\chi = \frac{IE + EA}{2} \qquad (1)$$

$$\eta = \frac{IE - EA}{2} \qquad (2)$$

According to Koopman's theorem,[16] the softness, σ, is the inverse of the hardness:[15]

$$\sigma = \frac{1}{\eta} \qquad (3)$$

The number of transferred electrons, ΔN, was also calculated by using the equation below:[16]

$$\Delta N = \frac{\chi_{Fe} - \chi_{inh}}{2(\eta_{Fe} + \eta_{inh})} \qquad (4)$$

Where χ_{Fe} and χ_{inh} denote the absolute electronegativity of Fe and inhibitor molecule, respectively, η_{Fe} and η_{inh} denote the absolute hardness of copper and inhibitor molecule, respectively. In this study, the theoretical values of $\chi_{Fe} = 7.0$ eV/mol and $\eta_{Fe} = 0$ eV/mol were used for the computation of a number of transferred electrons.[16] The absolute electrophilicity index is given by [17]

$$\omega = \frac{\mu^2}{2\eta} \qquad (5)$$

The total energy change was used to describe the energy change associated with the electron donation and electron back-donation processes that occurred during the adsorption process and are given by [18, 19]

$$\Delta E_{tot} = -\eta / 4 \qquad (6)$$

The degree of protonation was measured by calculating the proton affinity (PA) at each possible protonated site, for both inhibitors using **Error! Reference source not found.** [20]:

$$PA = E_{prot} + E_{H_2O} - E_{nuetral} - E_{H_3O^+} \qquad (7)$$

where E_{prot}, E_{H_2O}, $E_{nuetral}$ and $E_{H_3O^+}$ are the sum of electronic and thermal enthalpies of the protonated, water, neutral and hydronium ion, respectively.

Visual inspection was conducted using the Guassveiw programme (version 5.0.8) [21] and Chemcraft programme version 1.8 (build 489) [22].

2.2. Monte Carlo simulations (MCS)

The adsorption energies of the two corrosion inhibitors, namely, 2-aminobenzothiazole (ABT) and 2-mercaptobenzothiazole, were investigated to identify the lowest and most stable adsorption

configuration as they adsorbed to Fe surface. In this regard, MBThione's neutral form and ABT's protonated @N16 form were used in the simulation based on an analysis of the protonation state of the molecules in acidic aqueous solution using ACD/LABs commercial software, Percepta, licensed to KFUPM. The adsorption Locator module, in Material Studio version 7 from Biovia Accelrys, USA, was adopted for the MC simulation [23]. The Fe surface was built with a surface cleavage (110) using a 12 × 12 supercell with a slab thickness of 5 Å. The vacuum thickness was set to 40 Å to eliminate the effect of periodic boundary conditions on the system. A COMPASS (condensed phase optimized molecular potentials for atomistic simulation studies) force field was used for the simulation of all molecules and systems. A simulation of the corrosion inhibitor molecules MBThione and ABT on an Fe (110) surface was performed in order to locate the low energy adsorption sites of the molecules on the Fe surface.

3. RESULTS AND DISCUSSION

3.1. Intramolecular proton transfer tautomerization
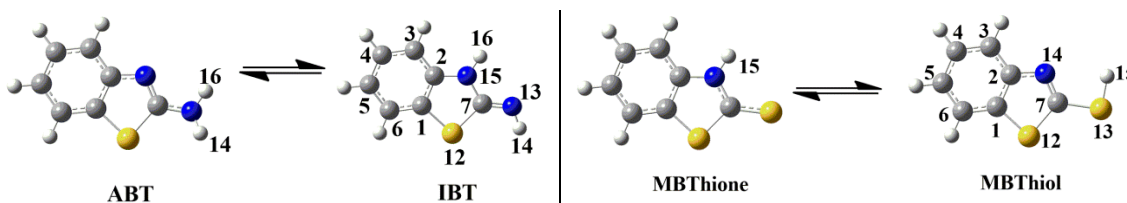
Figure 1. Optimized structures along with atomic numbering scheme of the tautomers of the investigated inhibitors

Table 1. Quantum chemical parameters (in eV) of ABT and IBT tautomers

	B3LYP				MP2			
	6-311++G(d,p)		6-311++G(3df,2p)		6-311++G(d,p)		6-311++G(3df,2p)	
QCPs	ABT	IBT	ABT	IBT	ABT	IBT	ABT	IBT
SCF energy (a.u.)	-778.19	-778.18	-778.23	-778.22	-776.55	-776.53	-776.82	-776.80
ΔE_{ele} (kcal/mol)	0.00	-6.04	0.00	-5.81	0.00	-9.41	0.00	-8.53
E_{HOMO}	-6.10	-5.93	-6.07	-5.90	-8.18	-8.08	-8.11	-8.01
E_{LUMO}	-0.78	-0.86	-0.75	-0.87	-1.04	-0.96	-1.02	-0.94
$E_L - E_H (HLG)$	5.33	5.06	5.32	5.03	7.14	7.12	7.10	7.07
Dipole moment	1.94	2.19	1.99	2.14	1.83	2.85	1.93	2.76
η	2.66	2.53	2.66	2.52	4.61	4.52	4.56	4.48
σ	0.38	0.40	0.38	0.40	0.22	0.22	0.22	0.22
χ	3.44	3.40	3.41	3.39	3.57	3.56	3.55	3.54
ΔN/e	0.67	0.71	0.67	0.72	0.37	0.38	0.38	0.39
ω/D^2.eV^{-1}	19.85	23.53	20.32	23.14	10.82	17.18	11.49	16.75
ΔE_T	-0.67	-0.63	-0.67	-0.63	-1.15	-1.13	-1.14	-1.12

Concerning the compounds under investigation, ABT and MBT, the type of side-chain tautomerism that relates to azole systems should be considered, containing exo-cyclic amino and thiol groups as proton donor groups [1]. The ABT compound can occur in two tautomeric forms: amino (2-aminobenzothiazole; ABT) and imino (2-iminobenzothiazole; IBT). Whereas the MBT compound can occur in two tautomeric forms: Thione (2-mercabtobenzothiazole; MBThione) and thiol (benzo[d]thiazole-2-thiol; MBThiol),

Figure 1.

Table 2. Quantum chemical parameters (in eV) of MBThione and MBThiol tautomers

QCPs	B3LYP				MP2			
	6-311++G(d,p)		6-311++G(3df,2p)		6-311++G(d,p)		6-311++G(3df,2p)	
	MBThione	MBThiol	MBThione	MBThiol	MBThione	MBThiol	MBThione	MBThiol
SCF energy (a.u.)	-1121.04	-1121.03	-1121.08	-1121.06	-1118.98	-1118.98	-1119.27	-1119.26
ΔE_{ele} (kcal/mol)	0.00	-8.74	0.00	-8.05	0.00	-3.87	0.00	-6.08
E_{HOMO}	-6.09	-6.47	-6.06	-6.44	-8.17	-8.44	-8.13	-8.39
E_{LUMO}	-1.63	-1.34	-1.61	-1.34	-0.81	-1.05	-0.81	-1.04
HLG	4.46	5.14	4.45	5.10	7.12	7.39	7.32	7.35
Dipole moment	5.03	0.86	4.88	0.83	5.65	0.97	5.49	0.89
η	2.23	2.57	2.22	2.55	4.49	4.75	4.47	4.71
σ	0.45	0.39	0.45	0.39	0.22	0.21	0.22	0.21
χ	3.86	3.91	3.84	3.89	3.68	3.70	3.66	3.6
ΔN / e	0.70	0.60	0.71	0.61	0.37	0.35	0.37	0.35
ω / $D^2.eV^{-1}$	61.40	9.12	59.72	8.81	34.19	5.54	33.44	5.13
ΔE_T	-0.56	-0.64	-0.56	-0.64	-1.12	-1.19	-1.12	-1.18

Since all four tautomeric forms are expected to coincide in solution, all are calculated. The analysis of two possible tautomers for ABT and MBThione are performed by the DFT/B3LYP and MP2, employing the 6-311++G(d,p) and 6-311++G(3df,2p) basis sets in the gas phase, from Table 1 and Table 2, respectively.

It has been reported that the equilibrium structure is entirely on the amino side of ABT. [1, 24] The calculated minimum energies for ABT and IBT tautomers in the gas phase show that the amino form (ABT) is lower in energy than the imino form (IBT) by 5.80 kcal/mol in the gas phase, for instance (Table 1 and

Figure 2), which suggests that the amino form is the primary constituent of this equilibrium. This finding is in agreement with results reported in the literature (a similar trend with 6.40 kcal/mol at the BPW91/6-31G(d,p) level in the gas phase) [1]. In contrast, it has been reported for the MBT compound that the equilibrium structure is almost entirely on the thione side [3]. The calculated

minimum energies for the MBThione and MBThiol tautomers show that the thione form (MBThione) is lower in energy than the thiol form (MBThiol) by 9.02 kcal/mol (Table 2 and

Figure 2), which suggests that the thione form is the major constituent of this equilibrium. This finding is in agreement with results reported in the literature [3]. The stability of MBThione over MBThiol nearly doubles the stability of ABT over IBT.

(a)   (b)
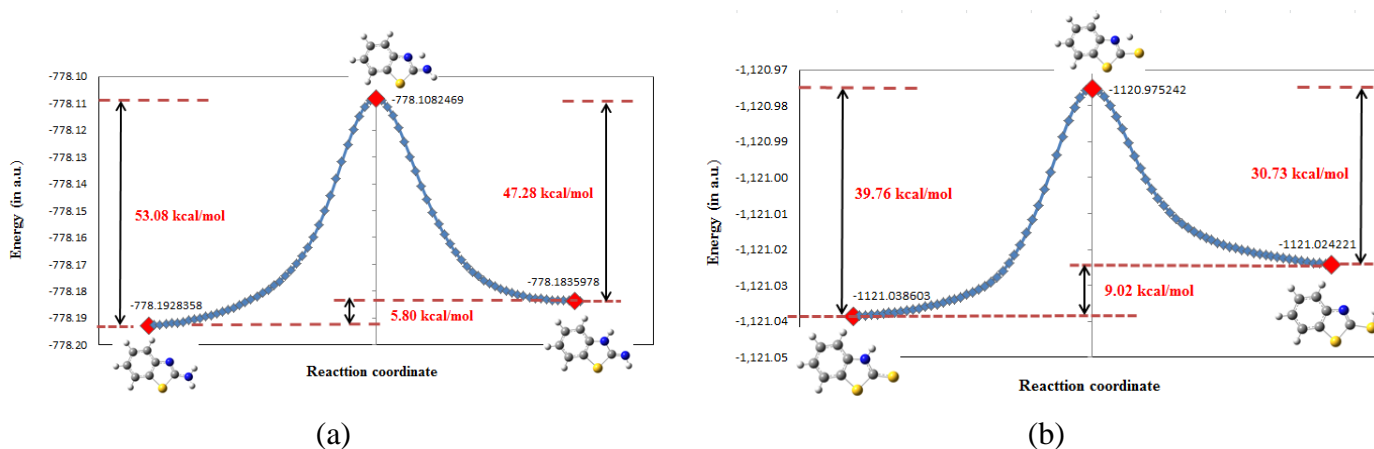
Figure 2. Potential energy curves of the tautomerization of (a) ABT → IBT and (b) MBThione → MBThiol

To further confirm that the amino and thione tautomers would be the main tautomers of the two investigated compounds, the intrinsic reaction coordinate (IRC) connecting the two minima tautomers and passing through a transition state (representing the minimum-energy connection pathway) was plotted for the two investigated compounds, see

Figure 2.

Figure 2 shows that the transition state (TS) connecting the two minima represents a maximum along the direction of the IRC. However, along all other directions it is a minimum, as evident from the frequency calculations, since only one imaginary frequency (IF) was obtained for each TS. The amino and thione forms are global minima, since they are the lowest energy minima on the entire 2D potential energy surface (PES), while their imino and thiol forms are relative minima.

To support the stability of different species of the two investigated tautomeric systems, *i.e.,* the ABT↔IBT and MBThione↔MBThiol interconversion, the kinetics, as well as the thermodynamics, of the tautomeric processes were calculated at B3LYP/6-311++G(d,p) in the gas phase, as shown in

Table 3. Results from

Table 3 indicate that the thermodynamic parameters, including the electronic energy change (corrected with the zero-point energy), ΔE_{ZPE}, the enthalpy change, ΔH, and the Gibbs free energy change, ΔG, between tautomers are represented. Additionally, kinetic parameters of the desired tautomeric interconversion are presented, including the activation energy, E_a, the energy barriers for the forward, $\Delta G_{fwd}^{\#}$, and backward, $\Delta G_{bwd}^{\#}$, of tautomeric reactions, the rate constants of the forward reactions, k_{fwd}, and reverse, k_{bwd}, and related equilibrium constants K_{eq} (the equilibrium constant for

a one-step reaction is equal to the forward rate constant divided by the backward rate constant), and the imaginary frequency and dipole moment of their corresponding TSs are also presented.

Table 3. Relative thermodynamic and kinetic data (in kcal/mol), rate constant (in s^{-1}), and equilibrium constant at 298.15K, imaginary frequency (in cm^{-1}) and dipole moment (in Debye) of the transition state for the tautomeric interconversion

Tautomeric interconversion	ΔE_{ZPE}[a]	ΔH[a]	ΔG[a]	E_a[b]	$\Delta G_{fwd}^{\#}$[c]	$\Delta G_{bwd}^{\#}$[c]	k_{fwd}[d]	k_{bwd}[d]	K_{eq}[e]	IF	DM
ABT↔IBT	5.96	5.91	5.80	53.35	49.08	43.29	6.44E-24	1.15E-19	5.59E-05	-1970	0.90
MBThione↔MBThiol	6.46	6.67	6.27	39.96	36.08	29.81	2.21E-14	8.76E-10	2.53E-05	-1703	3.46

[a] $\Delta E_{ZPE} = \Delta E_{ZPE}^{o}(P) - \Delta E_{ZPE}^{o}(R)$; [a] $\Delta H = \Delta H_{P}^{o} - \Delta H_{R}^{o}$; [a] $\Delta G = \Delta G_{P}^{o} - \Delta G_{R}^{o}$; [b] $E_a = E_{TS} - E_{R}$ (ABT/MBThio ne)

[c] $\Delta G_{fwd}^{\neq} = \Delta G(TS) - \Delta G$(ABT/MBThio ne); [c] $\Delta G_{bwd}^{\neq} = \Delta G(TS) - \Delta G$(IBT/MBThio l);

$$^{d} k_{fwd/bwd} = \frac{K_B T}{h} \exp^{(\Delta G_{fwd/bwd}^{\neq}/RT)}; \quad ^{e} K_{eq} = \frac{k_{fwd}}{k_{bwd}}$$

As evident from the positive values of ΔG, ABT and MBThione are the most stable tautomers with respect to their counterparts, IBT and MBThiol. Comparing the value of ΔG for the ABT→IBT process (5.801 kcal/mol) and for MBThione↔MBThiol (6.272 kcal/mol) indicates that the ABT→IBT process is not thermodynamically favourable compared to the MBThione→MBThiol process. Conversely, it can be observed that the activation barrier, E_a, of the ABT→IBT process is higher (53.347 kcal/mol) than that for the MBThione↔MBThiol process (39.963 kcal/mol). It could be concluded that from a kinetic point of view, the ABT→IBT process is more difficult than the MBThione↔MBThiol process. Moreover, the proton on the exo-cyclic sulphur could be transferred to the endo-cyclic nitrogen atom (in MBThione↔MBThiol) more easily than the proton transfer from the exo-cyclic nitrogen atom to the endo-cyclic nitrogen atom (in ABT→IBT). The imaginary frequencies of the transition states of the ABT↔IBT and MBThione↔MBThiol processes are -1970 and -1703 cm^{-1}, respectively. It is clear that the increase in the imaginary frequency's absolute value is combined with an energy barrier increase [25].

The K_{eq} values for the two tautomeric equilibriums are much smaller than unity and equal to 5.591 x 10^{-05} and 2.525 x 10^{-5} for ABT→IBT and MBThione→MBThiol, respectively. The values of K_{eq} are larger than those reported for the tautomerization process of selenobarbituric acid (< 1.63 x 10^{-6}) calculated at different functionals of DFT with the same basis set [25]. The K_{eq} value of the ABT→IBT tautomerism is twice that of the MBThione→MBThiol tautomerism. Therefore, the ABT and MBThione tautomers are the major tautomers in the gas phase, and the amounts of the other tautomers, IBT and MBThiol, are insignificant. However, the tautomerism rate constants are more important in those processes [25]. The calculated rate constants for the forward and backward reactions are extremely small, and these interconversions could not be observed at the gas phase. Thus, in the gas phase, they are thermodynamically unfavourable and could only occur under high thermal conditions, or by proton tunnelling. [25-27] However, it should be mentioned that the proposed

tautomerization pathway is only a unimolecular transition state for interconverting the amine, imines, or thione to thiol tautomers. Even for systems that can involve a nitrogen to nitrogen/sulphur proton transfer or *vice versa*, intramolecular TS that involve proton transfers through 4-atom-TS (bimolecular TS) would expect to result in considerably faster interconversions [27]. Additionally, it is worth noting that the rate constants for most intermolecular proton transfers in solvent-assisted models were intensively increased. Reported values show that such processes could be done in solvent-assisted models, and the less stable tautomers could be observed in these systems [25]. The calculated value of $\Delta G^{\#}_{fwd}$ for ABT interconversion to IBT (49.082 kcal/mol) is larger than that for MBThione interconversion to MBThiol (36.079 kcal/mol), which combined with the smaller value of k_{fwd} (6.441 x 10^{-24} s^{-1}) for ABT→IBT, can be compared to the value for MBThione→ MBThiol (2.211x 10^{-14} s^{-1}). However, for the values of $\Delta G^{\#}_{bwd}$ and k_{bwd}, the reverse trend was observed. The dipole moment values of the TSs are intermediate (0.901 D for the TS of ABT→IBT and 3.460 D for the TS of MBThione→ MBThiol interconversions) between the values of the minima tautomers. This finding indicates that the charges are redistributed during these interconversions [28].

Experimental inhibition efficiencies have been obtained by Jafari et al.[2]. According to these researchers' report, MBT's inhibition efficiency for steel corrosion was better than ABT's. In this regard, we used frontier molecular orbitals (FMO), HOMO and LUMO to predict the adsorption active site/s of the inhibitor molecule. DFT/B3LYP and MP2 methods with the 6-311++G(d,p) and 6-311++G(3df,2p) level of theory were adopted for these calculations. Table 1 and Table 2 summarize the calculated values of the FMO, *i.e.*, E_{LUMO}, and the energy gap of the tautomers of ABT and MBT, respectively. The adsorption process of the inhibitor on the metal surface increases with increasing HOMO energy (E_{HOMO}) and decreasing LUMO energy (E_{LUMO}). From the HOMO orbital, the inhibitor molecule will give electrons to the *d*-orbital of the metal molecule, and from the LUMO orbital, the inhibitor will accept the electrons from the *d*-orbital of the metal molecule; this process was defined as an electron-donation and electron-back-donation process. Thus, the electron donating ability of a molecule is often characterized by its E_{HOMO}, and a high value of E_{HOMO} indicates the tendency of the inhibitor to donate electrons to the acceptor Fe atoms. In contrast, E_{LUMO} indicates the ability of the inhibitor to accept electrons, and a lower value of E_{LUMO} indicates a greater tendency of the inhibitor to accept electrons from the donor metal [18, 29, 30]. It is expected that an inhibitor with larger inhibition efficiency has a higher HOMO energy (less negative value). The trend of increasing of HOMO energies is consistent with this prediction in all levels, except those calculated at MP2/6-311++G(3df,2p), *i.e.,* in the three levels, the order of increasing HOMO energy is E_{HOMO}(ABT) < E_{HOMO} (MBThione). Thus, MBThione, with the largest inhibition efficiency, has the higher HOMO energy. In contrast, the trend at which LUMO energies decrease (become more negative) with inhibition efficiencies at the four levels of theory behaves as expected. The LUMO energies decrease, *i.e.,* E_{LUMO} (ABT) > E_{LUMO} (MBThione), as the %IEs increase. This finding suggests that the electron-donation process from the inhibitor to the Fe surface and the electron back-donation process from the Fe surface to the inhibitor molecule are both competitive processes.

The HOMO-LUMO energy gaps increase in the following order: MBThione < ABT, with values ranging from 4.459 to 7.322 eV at the four levels of theory. We conclude that the high

inhibition efficiency of MBThione, when compared to ABT, is due to its smallest HOMO–LUMO energy gap (HLG). This is because, as HLG decreases, the reactivity of the molecule increases, leading to an increase in the strength of adsorption and hence in the inhibition efficiency.

Figure 3 shows the shapes of HOMO and LUMO orbitals of the inhibitors at the B3LYP/6-311++G(d,p). From this figure, it is evident that tautomers of the inhibitors are electron rich and are capable of donating electrons to the metal or oxide surface, which enhances their ability to inhibit iron corrosion, by forming an inhibition barrier [31].
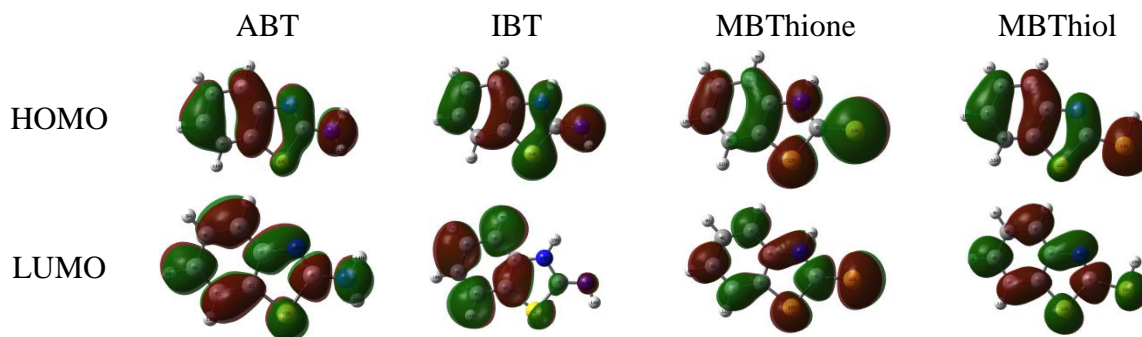
Figure 3. FMO distributions of the tautomer forms of the investigated inhibitors at the B3LYP/6-311++G(d,p) in the gas phase

The contribution of each donor/acceptor atom of ABT and MBT tautomers are calculated by a B3LYP method with 6-311++G(d,p) basis set, and the results are shown in Table 4. From the results, the regions of more significant electron density are localized around the more electronegative atoms, such as N13, N16, S12 and S13, and in π-regions. The contribution of the N13 atom has an energy of 24.43 eV the for IBT tautomer, while it is 18.09 eV for ABT, and this is due to the presence of the nitrogen lone pairs that increase the electron donating ability of the molecule. The N16 atom contributes an energy of 14.39 eV and 11.99 eV for IBT and ABT, respectively. Conversely, the N14 atom of MBThione is a less contributing donor atom than an N16 atom of ABT; this is due to the hydrogen bonding between N14 and H15, which reduces the energy of donating electrons. The highest values of an S12 atom acting as a donor atom follow the order, IBT > MBThione > MBThiol > ABT.

Table 4. Highest coefficients of the HOMO and LUMO of the tautomeric forms of ABT and MBT at the B3LYP/6-311++G(d,p) in the gas phase

	Atomic numbering						
	Maximum coefficient of the HOMO						
	C1	C2	C7	S12	S13	N13	N16/N14
ABT	12.84	13.15	9.46	2.17	–	18.09	11.99
IBT	10.99	9.82	0.63	17.33	–	24.43	14.39
MBThione	6.98	6.46	1.02	14.40	47.80	–	9.17
MBThiol	11.60	12.62	8.49	2.54	30.67	–	7.45
	Maximum coefficient of the LUMO						
ABT	1.82	12.62	22.63	6.33	–	5.04	3.75
IBT	14.23	2.00	1.21	2.16	–	1.49	0.07

| MBThione | 0.38 | 3.75 | 31.30 | 6.59 | 22.42 | – | 3.94 |
| MBThiol | 3.22 | 7.83 | 29.47 | 8.48 | 6.29 | – | 9.48 |

The terminal sulphur atom (S13) of MBThione is shown as the highest donor atom at 47.80 eV, whereas MBThiol only has 30.67 eV of energy to donate here. The C1 and C2 atoms have HOMO energy values of between 13.15 eV and 6.46 eV. The order of the highest values of C1 and C2 atoms (as donor atoms) is ABT > MBThiol > IBT > MBThione. The highest value of HOMO energy for the C7 atom is found in the ABT form, while the IBT form has the lowest value. The C7 atom of MBThione can donate approximately 1.02 eV of energy. The lower energy the acceptor atom is, the higher its LUMO value energy is.

The N16 atom of the IBT form has more of an ability to accept electrons than that of its ABT form; this property can be attributed to the hydrogen bonding between N16 and H15. The N14 atom of MBThione has a lower value of LUMO energy (3.94 eV) compared to MBThiol (9.48 eV). The S13 atom of MBThiol accepts electrons more than in MBThione by 16.13 eV. The C1 atom of MBThione accepts electrons more than the ABT tautomer. However, the C2 atom accepts electrons as in the following order: IBT > MBThione > MBThiol > ABT. The ability of an S12 atom to accept electrons is equal for the MBThione and ABT tautomers. In general, the two sulphur atoms of MBThione contribute an energy of 62.2 eV, while the contribution of the two nitrogen atoms in ABT equal to 30.08 eV.

The analysis of the QCPs at the four levels of theory will be restricted to the most stable tautomers of the investigated inhibitors, *i.e.,* ABT and MBThione. The dipole moment (μ) is an important electronic parameter that results from an unequal distribution of charges on the different atoms in a molecule. A large dipole moment may increase the adsorption of an inhibitor on a metal surface [32]. The energy of deformability increases with an increase in μ, thus, the molecule will be easier to adsorb at the iron surface. In addition, increasing μ increases the volume of the inhibitor molecules; this increases the contact area between the inhibitor and the surface of the iron and increases the corrosion inhibition ability of the inhibitor. In our study, MBThione has larger dipole moments than ABT in all levels of theory. This finding indicates MBThione's better inhibition efficiency compared to ABT, which entirely agrees with the experimental findings in Table 1 and Table 2.

Chemical hardness (η) and softness (σ) are significantly related to the band gap (HLG). They are important properties to measure the stability and reactivity of a molecule. It is apparent that chemical hardness shows a resistance towards the polarization or deformation of the electron cloud of atoms, ions, or molecules by the small perturbations of a chemical reaction. A soft molecule has a small energy gap and a hard molecule has a large energy gap [33]. According to Pearson, hard molecules with large energy gaps cannot act as good corrosion inhibitors [34]. Conversely, soft molecules with small energy gaps are efficient corrosion inhibitors because they can easily donate electrons to metal atoms at the surface. For instance, at the B3LYP/6-311++G(d,p), the chemical softness values of ABT and MBThione are 0.376 and 0.449 eV, respectively. As a result, MBThione is a softer molecule than ABT, while their hardness values follow the opposite trend. Since the number of heteroatoms in the two molecules is the same, the presence of two sulphur atoms and one nitrogen atom in the MBThione molecule make it softer, compared to the presence of two nitrogen atoms and

one sulphur atom in ABT molecule. The electronegativity (χ), which is the negative of the chemical potential (μ), also indicates the propensity of an inhibitor molecule to accept electrons/electron density towards itself when cooperating with iron atoms in a complex. The higher the electronegativity of a molecule, the stronger its adsorption on an iron surface. Table 1 and Table 2 show the order of electronegativity as MBThione > ABT. Hence, an increase in the difference of electronegativity between the iron and an inhibitor is observed in the order MBThione > ABT. For instance, at the B3LYP/6-311++G(d,p), the electronegativity values of ABT and MBThione are 3.439 and 3.859 eV, respectively. According to Sanderson's electronegativity equalization principal [35], MBThione, with a large electronegativity and a small difference of electronegativity, rapidly reaches equalization. Hence, its reactivity is expected to be high, which, in turn, indicates high inhibition efficiency; another conclusion in total agreement with the experimental finding.

The electrophilicity index (ω) is a quantum chemical descriptor that represents the propensity of an inhibitor molecule to accept an electron [17]. The electrophilicity values of the two benzothiazole compounds range from 10.818 to 61.404 D^2/eV at the four levels of theory. According to this descriptor, the electron-receiving capacity of the MBThione is significantly larger than that of the ABT molecule. For instance, at the B3LYP/6-311++G(d,p), the electrophilicity values for ABT and MBThione are 19.853 and 61.404 D^2/eV, respectively. This trend is similar to those seen for the softness and electronegativity, as revealed above. Generally, MBThione, containing more sulphur atoms, accepts electrons more easily than ABT, containing more nitrogen atoms. Thus, according to the descriptors evaluated in this section, the type and number of heteroatoms significantly influences the reactivity of the benzothiazole derivative, and can be used to predict the inhibition effect of the derivative [36]. Actually, the exo-cyclic sulphur atom in MBThione causes the electron density on the benzothiazole ring to increase, enhancing the electron-releasing capacity of the molecule. In contrast, the exo-cyclic nitrogen atom in the ABT molecule causes the electron density on the benzothiazole ring to decrease (although, sulphur is less electronegative than nitrogen). By analysing the Mulliken population charges later in Section 3.7, we will show that the exo-cyclic sulphur atom carries more negative charge at the four electronic states of MBThione than the exo-cyclic nitrogen in the ABT molecule.

Furthermore, Table 1 and Table 2 include the values of the number of electrons transferred (ΔN). The iron surface and an inhibitor molecule are two systems with different electronegativities. It is expected that the following mechanism will occur: the equilibrium chemical potential is reached by a flow of the electrons from the inhibitor molecule (with lower electronegativity) to the iron surface (with higher electronegativity). The ΔN values do not specify the exact number of electrons that exit the donor and arrive at the acceptor molecule. Thus, the expression "electron-donating ability" has been recommended to be more suitable than "number of electron transferred" [31, 37]. For the values of $\Delta N < 3.6$, the inhibition efficiency of an inhibitor increases as a result of an increase in the electron releasing ability at the iron surface [37]. The level of theory that was able to satisfy this relationship was the B3LYP with two basis sets, while the MP2 with the two basis sets was not able to establish this relationship. The MP2 method gives very comparable values of the ΔN values, with a difference of 0.002-0.005 e, while the ΔN values of MBThione are significantly larger than those of ABT, by no less than 0.035 e.

In an acidic medium, the benzothiazole derivatives predominantly act as bases and attract protons because of the existence of heteroatoms with lone pairs of electrons. For this reason, all of the possible sites for the protonation process were calculated, *i.e.,* the N13, N14, N16, S12 and S13 atoms of the two investigated inhibitors. The stability data for the neutral and protonated forms of the investigated inhibitors at the B3LYP/6-311++G(d,p) level of theory in the gas phase are summarized in Table 5. Note that the protonation at the endo-cyclic S12 in the four tautomers, ABT, IBT, MBThione, and MBThiol, results in the opening of the thiazole ring, meaning that the structure of the molecule is completely distorted. Thus, protonation at this site is neglected.

Table 5. Relative energies (in kcal/mol), the sum of the electronic and thermal enthalpies (in a.u.) and proton affinities (in kcal/mol) for neutral and the possible protonated forms of the ABT, IBT, MBThione, and MBThiol

Tautomer	Form	RE	$E_{ele} + H$	PA	Tautomer	Form	RE	$E_{ele} + H$	PA
ABT	Neutral	-232.48	-778.07	−	MBThione	Neutral	-217.57	-1120.93	−
	PN13	-25.95	-778.38	-26.37		PN14	-26.45	-1121.22	-11.83
	PN16	0.00	-778.42	-53.09		PS13	0.00	-1121.26	-40.20
IBT	Neutral	-238.52	-778.06	−	MBThiol	Neutral	-224.77	-1120.92	−
	PN13	0.00	-778.42	-59.00		PN14	0.00	-1121.26	-45.42
	PN16	-36.84	-778.36	-21.99		PS13	-39.89	-1121.20	-7.47

The results in Table 5 show that for the protonated form, a more stable structure is obtained compared to the neutral form, and this follows the trend, ABT P@N16 > IBT P@N13 > ABT P@N13 > IBT P@N16 > ABT > IBT, while the trend for the other molecule is MBThione P@S13 > MBThiol P@N14 > MBThione P@S13 > MBThiol P@S13 > MBThione > MBThiol.

Table 6. Calculated QCPs for the most stable protonated forms of the tautomers at the B3LYP/6-311++G(d,p) in the gas phase, regular font, and aqueous solution, bold font

Inhibitor	E_{HOMO} /eV	E_{LUMO} /eV	HLG /eV	η /eV	χ /eV	ω / D^2.eV^{-1}	μ /D	ΔE_{tot} /eV	ΔN /e
ABT(PN16)	-10.776	-5.647	5.129	2.565	8.212	59.703	5.627	-0.641	-0.236
	-7.137	**-1.757**	**5.380**	**2.690**	**4.447**	**80.898**	**7.997**	**-0.673**	**0.475**
IBT(PN13)	-10.776	-5.647	5.129	2.565	8.212	59.702	5.627	-0.641	-0.236
	-7.137	**-1.757**	**5.380**	**2.690**	**4.447**	**80.896**	**7.997**	**-0.673**	**0.475**
MBThione(PS13)	-11.066	-6.511	4.555	2.278	8.789	22.239	1.861	-0.569	-0.393
	-7.400	**-2.681**	**4.719**	**2.360**	**5.041**	**36.694**	**3.182**	**-0.590**	**0.415**
MBThiol(PN14)	-11.064	-6.515	4.549	2.275	8.789	37.933	3.171	-0.569	-0.393
	-7.399	**-2.683**	**4.715**	**2.358**	**5.041**	**52.526**	**4.551**	**-0.589**	**0.415**

To confirm the true protonated forms of the two molecules, ACD/Lab software was used. This showed that the protonation of ABT in acidic media occurred at the N16 site. In contrast, the MBThione form is not protonated at all, while the MBThiol form is protonated at the N14 site.

The 2D and 3D maps of molecular electrostatic potential (MESP) reflect the electronic density distributions within the molecule. In

Figure 4, one can see the MESP maps of the ABT, IBT, MBThione, and MBThiol tautomers, as well as the protonated forms of the most stable tautomers at the most stable protonated sites, *i.e.,* ABT P@N16 and MBThione P@S13. Blue and red parts in the MESP 3D map represent regions of positive and negative potential and correspond to the electron-poor and electron-rich regions, respectively, while the green coloured parts represent neutral electrostatic potential [4, 38]. The MESP contains information about all the electronic components of the molecule, and describes regions of electrophilicity and nucleophilicity on the surface of a molecule [38].
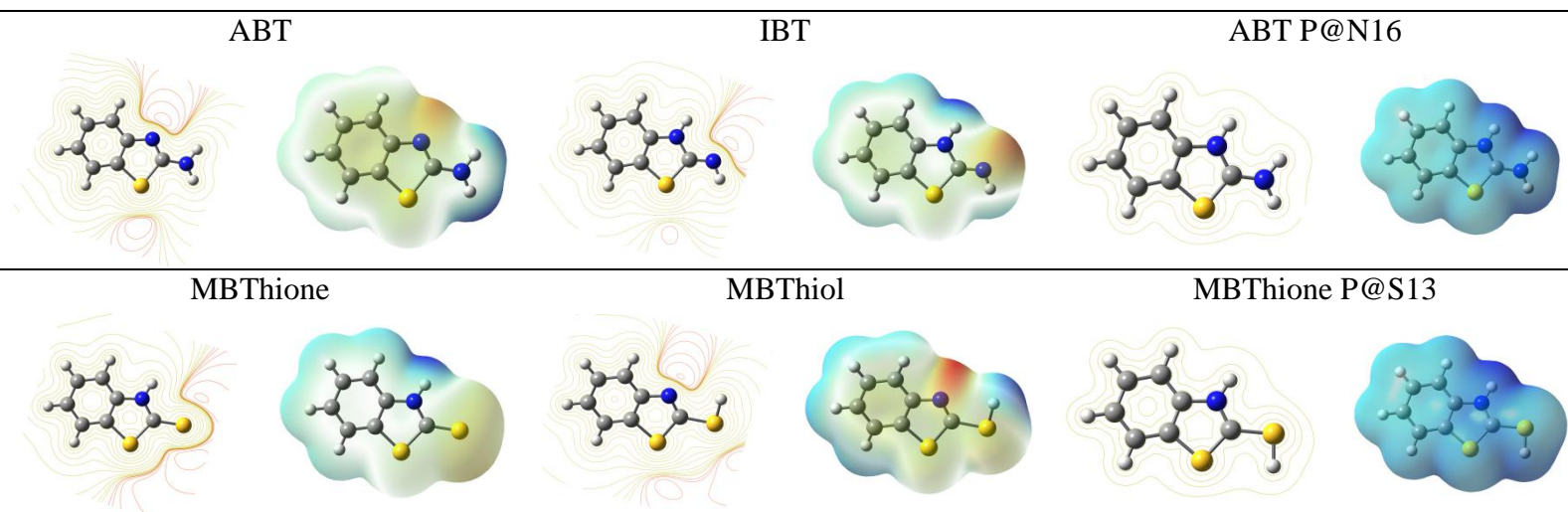
Figure 4. Electrostatic properties of ABT, IBT, ABT P@N16, MBThione, MBThiol, and MBThione P@S13: 2D contour map and 3D MESP surface at the B3LYP/6-311++G(d,p) in the gas phase

A 3D plot of the MESP surface of the ABT tautomer shows that the endo-cyclic nitrogen atom (N16) with a high electron density region is most likely to receive a proton. For the IBT tautomer, MESP confirms that the exo-cyclic nitrogen atom (N13) of IBT is the most likely to be protonated. Thus, it is the regions with negative potential values that are most attracted to approaching protons. This leads to the previously calculated stability patterns of the different protonated forms of these two tautomers. Similar treatment could be applied to the MESP plots of the MBThione and MBThiol tautomers. The region of highest electron density is found around the exo-cyclic sulphur atom (S13) in MBThione and around the endo-cyclic nitrogen atom (N14) in MBThiol. Moreover, it can be seen that the negatively charged regions are delocalized on the benzene ring in the ABT, IBT and MBThiol tautomers. The benzene rings in these tautomers are electron-rich areas that would be the favoured sites for adsorption to an iron surface. The 2D MESP contour maps plotted in

Figure 4 provide complete information concerning MESP distributions, by showing them in a multitude of spatial position around the molecules.

3.2. Chemical and physical adsorption of the inhibitor on Fe surface

In the chemical model, a chemical bond is presumed to be formed by releasing electrons from the filled HOMO of the inhibitor molecules into the empty *d*-orbitals of iron atoms. It is also possible that back-bonding can result through electron donation from the filled metal d-orbitals to the vacant LUMO of the inhibitor [6]. E_{HOMO}, E_{HOMO}, and their energy gaps are calculated for the ground electronic states (S$_o$), excited electronic states (S$_1$), cationic ground states (S_o^+), anionic ground states (S_o^-) and most stable protonated states, *i.e.,* ABT P@N16 and MBThioneP@S13, Table 7. Correlation is established by comparing the calculated quantum chemical parameters with inhibition efficiency.

Table 7. FMO parameters (in eV) for four electronic states of ABT and MBThione at the B3LYP/6-311++G(d,p) in the gas phase

	ABT				MBThione			
	S$_o$	S$_1$	S_o^+	P@N16	S$_o$	S$_1$	S_o^+	P@S13
E_{HOMO}	-6.10	-6.10	-11.43	-10.78	-6.09	-6.09	-11.51	-11.07
E_{LUMO}	-0.78	-0.78	-5.96	-5.65	-1.63	-1.63	-6.57	-6.51
EG	5.33	5.33	5.47	5.13	4.46	4.46	4.94	4.56

The best correlation between the inhibition efficiency and E_{HOMO} was found for S_o and S_1, *i.e.,* the HOMO energy for the more efficient inhibitor (MBThione) was determined to be higher than that of the less efficient inhibitor (ABT). This finding implies that S_o and S_1 can be equally responsible for the bonding between an inhibitor and the *d*-orbitals of iron ions to make a chemical bond between them. In contrast, the relationship between the inhibition efficiency and the E_{LUMO} of the two inhibitors shows that the best correlations are with the four electronic states. In other words, the LUMO energy, for the more efficient inhibitor (MBThione), was found to be lower than that of the less efficient inhibitor (ABT), indicating that back bonding was achieved by an equal donation of electrons from the iron ion's filled *d*-orbitals to the inhibitor LUMO's empty orbitals for the four electronic states of the inhibitor.

Similarly, Table 7 shows the correlation between the inhibition efficiency and EG for the two inhibitors in S_o, S_1, S_o^+, and the ABTP@N16 and MBThioneP@S13 states. Table 7 shows that the best correlation was found with the four electronic states, *i.e.,* the energy gap for the more efficient inhibitor (MBThione) was found to be smaller than that of the less efficient inhibitor (ABT) [6].

In the physical adsorption model, an electrostatic attraction is assumed between the corrosion inhibitor and the Fe surface. Apparently, the atomic charges on the heteroatoms of the inhibitors can be used as an index to account for physical adsorption. In this model, the molecule with the largest atomic charge on a heteroatom will have a higher tendency towards physical adsorption on the metal surface [6]. The charge distribution on a molecule might reasonably be taken as an indication for locating the positions of interaction between the inhibitor and the metal surface. Based on Mulliken population analysis, which partitions the total atomic charge among the atoms in a molecule, the total atomic charges on the different atoms for the inhibitor molecules have been obtained, see

Figure **5**. Mulliken population analysis is a random scheme for assigning charges. Atomic charges are not quantum mechanical observables and are ambiguously predicted from the first

principles. Calculated atomic charges for the optimized structures of inhibitor molecules in four electronic states (S_o, S_o^+, S_o^-, and protonated@N16 in ABT and @S13 in MBThione) are shown in

Figure **5**, which also shows the direction of the dipole moment vector. The Mulliken population charge analysis of the four electronic states of an ABT molecule shows that the exo-cyclic nitrogen atom (N13) has excess negative atomic charge, compared to both the endo-cyclic nitrogen atom (N16) and the endo-cyclic sulphur atom (S12). This result is contrary to the electron density distribution, as demonstrated by the 3D and 2D plots of MESP.

In contrast, for the MBThione molecule, the exo-cyclic sulphur atom (S13) has excess negative atomic charge compared to both the endo-cyclic nitrogen atom (N14) and the endo-cyclic sulphur atom (S12). This finding explains the stability of the protonated forms at these two sites for the molecules compared to the stabilities of the protonated forms at the other sites, as demonstrated in Section 3.4.

	S_o	S_o^+	S_0^-	P@N16/S13
ABT				
MBThione				
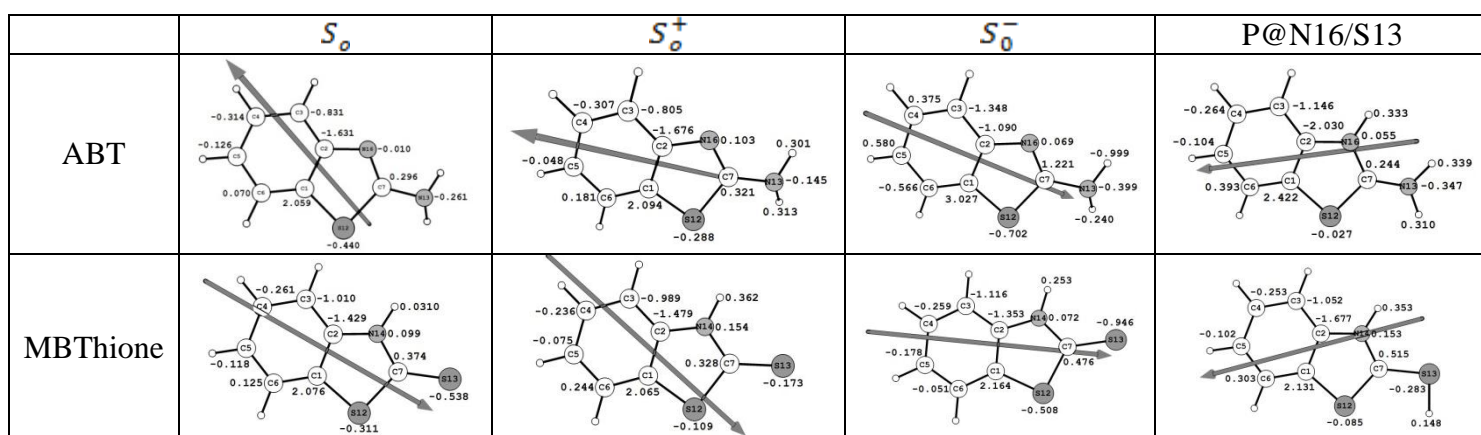
Figure 5. Mulliken atomic charges on the different atoms of the four electronic states of the optimized geometries of inhibitors molecules at the B3LYP/6-311++G(d,p), Note: arrows show the direction of dipole moment.

From an analysis of the atomic charges on the heteroatoms of the two inhibitors in different electronic states, it has been observed that the physical adsorption model is sufficient to account for the experimental findings based solely on the electrostatic attraction between the heteroatom and the positively charged metal atom surface. The atomic charges on heteroatom S12 in both inhibitors and N13 (in ABT) and S13 (in MBThione) in the S_o state are negatively charged with a charge ranging from -0.027 e to -0.508 e. Similar results are observed for the two inhibitors in various electronic states. For example, the recorded atomic charges for S12, ABT and MBThione are, respectively, -0.440 and -0.311 e in the S_o state, -0.288 and -0.109 e in the S_o^+ state, -0.702 and -0.508 e in the S_o^- state, and -0.027 and -0.085 e in the P@N16/S13 state. Correlation with the physical mode shows that the inhibition efficiency is arranged as follows: MBThione > ABT. Therefore, this suggests that MBThione is the most effective corrosion inhibitor, a result which is in agreement with the experimental findings [2].

Inhibitors exert their action by hindering the cathodic reaction in addition to stimulating the anodic process of metal dissolution through the formation of a barrier layer by blocking the reaction sites [6, 39]. Please note that it has been reported that benzothiazole and its derivatives are efficient

cathodic inhibitors, influencing the kinetics of hydrogen evolution [40], and that potentiodynamic polarization curves show that ABT behaves as a mixed-type corrosion inhibitor by inhibiting both cathodic reactions and anodic metal dissolution [1, 5]. From the adsorption of the ABT inhibitor on a steel surface in acidic solution, Danaee et al. [1] concluded that as observed from Langmuir adsorption isotherms and from the thermodynamic parameters of adsorption, the adsorption of ABT involves both chemical and physical adsorption. The quantum calculations given in the present report supports the mixed mode of adsorption, *i.e.*, chemisorption preceded by physisorption, a result that is consistent with the conclusions derived in the literature. [1]

3.3. Modelling of inhibitor-iron interaction using Monte Carlo simulations

The interaction between the two corrosion inhibitors (MBThione and ABT), protonated @N16, and the Fe (110) surface was investigated in order to locate the low energy adsorption configuration and the electron transfer process that occurs at the steel/electrolyte interface. The output of the Monte Carlo simulation for the adsorption of MBThione and ABT on the Fe (110) surface is presented in Table 8. Furthermore,

Figure **6** shows the snapshot of the top views for the adsorption of (a) MBThione and (b) ABT on the Fe (110) surface using a Monte Carlo simulation.

Table 8. Output of Monte Carlo simulation for the adsorption of MBThione and ABT on Fe (110) surface (in kJ/mol)

System	E_{tot}	E_{ads}	E_{rigid}	E_{def}	dE_{ads}/dN_i
Fe (110) + MBThione	-251.74	-345.16	-347.17	2.01	-345.16
Fe (110) + ABT	-57.57	-330.87	-332.55	1.63	-330.87

| (a) | (b) |
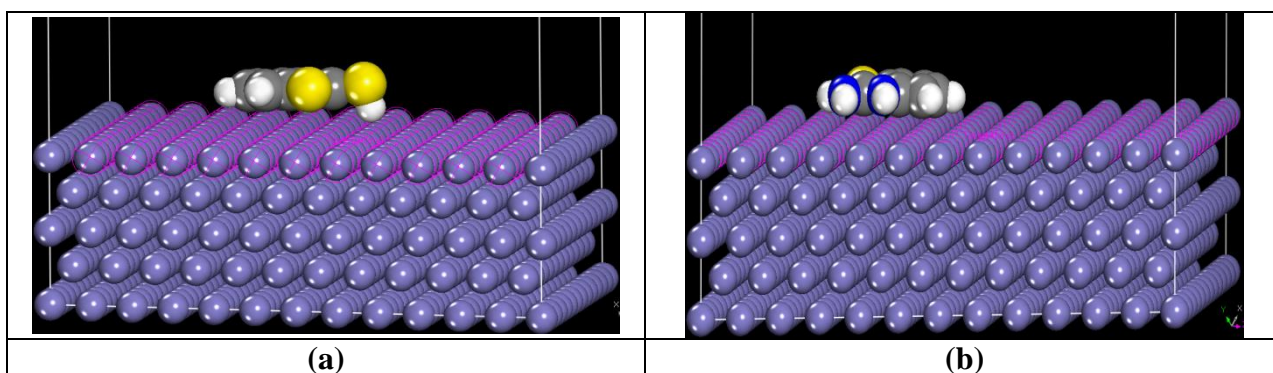
Figure 6. Snapshot of the top views for the adsorption of (a) MBThione and (b) ABT on an Fe (110) surface using Monte Carlo simulation.

The present study was performed using three cycles of simulated annealing with 10,000 steps for each process. The temperature of the annealing process was set automatically at 10^5 to 10^2 K for each cycle. Possible adsorption configurations were obtained as the temperature was slowly decreased

(simulated annealing procedure). The output of the simulations includes the total energy (E_{tot}), the adsorption energy (E_{ads}), the rigid adsorption energy (E_{rigid}), the deformation energy (E_{def}), and the differential adsorption energy (dE_{ads}/dN_i). The definitions and meanings of the various output parameters has been documented previously [41].

The equilibrium adsorption configurations of MBThione and ABT with a stable Fe (110) crystallographic plane are presented in

Figure **6**. As seen in

Figure **6**, both MBThione and ABT are adsorbed in a parallel orientation to the metal's surface. Furthermore, the N and S heteroatoms of both inhibitors adsorbed closer to the metal surface in a parallel orientation. This maximizes contact with the steel surface and enhances their adsorption on it. The extra S atom in MBThione could be the reason for the high adsorption energy of MBThione when compared to ATB. Additionally, the stability of MBThione in acidic media is another reason for its strong adsorption onto the steel surface. MBThione exists in its neutral form in acidic media; therefore, its N and two S atoms have excess electrons for binding to the metal surface. In contrast, ABT is protonated in acidic media, and so it is unstable and has fewer electrons to donate to the Fe (d) orbitals. According to Table 8, MBThione has higher negative adsorption energy than ABT. It has been reported that the higher the negative adsorption energies, the stronger the interaction of inhibitor molecules with metal surfaces [42-45]. Moreover, from Table 8, ABT is more deformed than MBThione, which supports the idea that the MBThione is more stable than ABT.

We conclude from the results obtained that the interaction between MBThione and a steel surface is stronger than that for ABT. This indicates that MBThione is expected to inhibit steel corrosion in 1 M HCl solution better than ABT. Thus, the theoretical results are in good agreement with the experiment.

4. CONCLUSIONS

The mechanism of corrosion inhibition for two well-known corrosion inhibitors, 2-aminobenzothiazole (ABT) and 2-mercaptobenzothiazole (MBThione), for steel in acidic media has been investigated from an atomic level of understanding. Quantum chemical calculations and Monte Carlo simulations were the theoretical tools adopted for this study. Quantum chemical calculations were performed using two methods (B3LYP and MP2), and two basis sets (6-311++G(d,p) and 6-311++G(3df,2p)) were used to calculate the electronic properties of the two molecules and their different tautomeric and protonated forms. The results from the experiments performed in this paper can be summarized into the following four points:

- The two inhibitors can exist in different tautomeric forms and can be protonated at different positions.

- The quantitative quantum chemical parameters were correlated with experimentally determined inhibition efficiencies.

- The quantum calculations given in the present report supports the mixed mode of adsorption, *i.e.*, chemisorption preceded by physisorption.

- Monte Carlo simulations found the equilibrium adsorption configurations and computed the adsorption energies between the diazole corrosion inhibitors and the Fe surface.

These results indicate that the adsorption energies follow the order: MBThione > ABT. The efficiency order and the mechanism of action for the studied inhibitors on a steel surface, as obtained by experimental results, have thereby been verified by theoretical calculations.

ACKNOWLEDGEMENT

References

1. I. Danaee, M. Gholami, M. RashvandAvei and M.H. Maddahy, *Journal of Industrial and Engineering Chemistry*, 26 (2015) 81.
2. H. Jafari, K. Akbarzade and I. Danaee, *Arabian Journal of Chemistry*, (2014).
3. T.L.P. Galvão, A. Kuznetsova, J.R.B. Gomes, M.L. Zheludkevich, J. Tedim and M.G.S. Ferreira, *Theoretical Chemistry Accounts*, 135 (2016) 78.
4. M. Dehdab, M. Shahraki and S.M. Habibi-Khorassani, *Iranian Journal of Science and Technology (Sciences)*, 39 (2015) 311.
5. P.B. N. S. Patel, M. Nebyla, M. Přibyl, D. Šnita, *International Journal of ELECTROCHEMICAL SCIENCE*, 9 (2014) 3951.
6. M.E. Elshakre, H.H. Alalawy, M.I. Awad and B.E. El-Anadouli, *Corrosion Science*, 124 (2017) 121.
7. E.E. Oguzie, C.B. Adindu, C.K. Enenebeaku, C.E. Ogukwe, M.A. Chidiebere and K.L. Oguzie, *The Journal of Physical Chemistry C*, 116 (2012) 13603.
8. M.E. Belghiti, S. Bouazama, S. Echihi, A. Mahsoune, A. Elmelouky, A. Dafali, K.M. Emran, B. Hammouti and M. Tabyaoui, *Arabian Journal of Chemistry*, (2017).
9. S. Kaya, B. Tüzün, C. Kaya and I.B. Obot, *Journal of the Taiwan Institute of Chemical Engineers*, 58 (2016) 528.
10. Ş. Erdoğan, Z.S. Safı, S. Kaya, D.Ö. Işın, L. Guo and C. Kaya, *Journal of Molecular Structure*, 1134 (2017) 751.
11. M.J. Frisch, Gaussian 09 Programmer's Reference, Gaussian, 2009.
12. A.D. Becke, *Physical Review A*, 38 (1988) 3098.
13. C. Lee, W. Yang and R.G. Parr, *Physical Review B*, 37 (1988) 785.
14. M. Head-Gordon and T. Head-Gordon, *Chemical Physics Letters*, 220 (1994) 122.
15. R.G. Parr and R.G. Pearson, *Journal of the American Chemical Society*, 105 (1983) 7512.
16. R.G. Pearson, *Inorganic Chemistry*, 27 (1988) 734.
17. R.G. Parr, L.s.v. SzentpÃ¡ly and S. Liu, *Journal of the American Chemical Society*, 121 (1999) 1922.
18. E.E. Ebenso, T. Arslan, F. Kandemirlı, I. Love, C.l. Öğretır, M. Saracoğlu and S.A. Umoren, *International Journal of Quantum Chemistry*, 110 (2009) 2614.
19. B. Gomez, N.V. Likhanova, M.A. Dominguez-Aguilar, R. Martinez-Palou, A. Vela and J.L. Gasquez, *The Journal of Physical Chemistry B*, 110 (2006) 8928.
20. B. El Ibrahimi, A. Soumoue, A. Jmiai, H. Bourzi, R. Oukhrib, K. El Mouaden, S. El Issami and L. Bazzi, *Journal of Molecular Structure*, 1125 (2016) 93.
21. Roy Dennington, T. Keith and J. Millam, GaussView, in: S. Mission (Ed.), *Semichem Inc.*, KS, 2009.
22. G. Zhurko and D. Zhurko, Chemcraft program, Academic version 1.8, 2009.
23. R.L.C. Akkermans, N.A. Spenley and S.H. Robertson, *Molecular Simulation*, 39 (2013) 1153.

24. L. Forlani and P. De Maria, *Journal of the Chemical Society, Perkin Transactions 2*, (1982) 535.
25. H. Tavakol and F. Keshavarzipour, *Structural Chemistry*, 26 (2015) 1049.
26. N. Wazzan and Z. Safi, *Journal of Molecular Structure*, 1143 (2017) 397.
27. C.S. Tautermann, A.F. Voegele and K.R. Liedl, *Chemical Physics*, 292 (2003) 47.
28. N. Wazzan and Z. Safi, *Journal of Molecular Structure*, 1143 (2017) 397.
29. G. Gece and S. Bilgic, *Corrosion Science*, 51 (2009) 1876.
30. N.A. Wazzan, I.B. Obot and S. Kaya, *Journal of Molecular Liquids*, 221 (2016) 579.
31. I.B. Obot, D.D. Macdonald and Z.M. Gasem, *Corrosion Science*, 99 (2015) 1.
32. X. Li, S. Deng, H. Fu and T. Li, *Electrochimica Acta*, 54 (2009) 4089.
33. N. O. Obi-Egbedi, I. B. Obot, M. I. El-khaiary, S. A. Umoren and E.E. Ebenso, *International Journal of ELECTROCHEMICAL SCIENCE*, 6 (2011) 5649.
34. R.G. Pearson, *Coordination Chemistry Reviews*, 100 (1990) 403.
35. P. Geerlings and F.D. Proft, *Int. J. Mol. Sci.*, 3 (2002) 276.
36. D.Q. Dao, T.D. Hieu, T. Le Minh Pham, D. Tuan, P.C. Nam and I.B. Obot, *Journal of Molecular Modeling*, 23 (2017) 260.
37. I. Lukovits, E. Kálmán and F. Zucchi, *CORROSION*, 57 (2001) 3.
38. N. Karakus and K. Sayin, *Journal of the Taiwan Institute of Chemical Engineers*, 48 (2015) 95.
39. A.E. Stoyanova, E.I. Sokolova and S.N. Raicheva, *Corrosion Science*, 39 (1997) 1595.
40. M.A. Quraishi, M.A. Wajid Khan, M. Ajmal, S. Muralidharan and S. Venkatakrishna Iyer, *Journal of Applied Electrochemistry*, 26 (1996) 1253.
41. F. El-Taib Heakal, S.A. Rizk and A.E. Elkholy, *Journal of Molecular Structure*, 1152 (2018) 328.
42. I.B. Obot, S.A. Umoren, Z.M. Gasem, R. Suleiman and B.E. Ali, *Journal of Industrial and Engineering Chemistry*, 21 (2015) 1328.
43. A. Madhan Kumar, R. Suresh Babu, I.B. Obot and Z.M. Gasem, *RSC Advances*, 5 (2015) 19264.
44. M. El Faydy, M. Galai, M.E. Touhami, I.B. Obot, B. Lakhrissi and A. Zarrouk, *Journal of Molecular Liquids*, 248 (2017) 1014.
45. L.Guo, I.B.O. G. Ye, X. Li, X. Shen, W. Shi and X. Zheng, *International Journal of Electrochemical Sceince*, 12 (2017) 166.